Near-infrared-emissive polymersomes: Self-assembled soft matter for *in vivo* optical imaging

P. Peter Ghoroghchian*†, Paul R. Frail†, Kimihiro Susumu†, Dana Blessington‡, Aaron K. Brannan§, Frank S. Bates§, Britton Chance‡, Daniel A. Hammer*¶, and Michael J. Therien†¶

*School of Engineering and Applied Science, Institute for Medicine and Engineering, †Department of Chemistry; and ‡Johnson Research Foundation, Department of Biochemistry and Biophysics, School of Medicine, University of Pennsylvania, Philadelphia, PA 19104; and §Department of Chemical Engineering and Materials Science, University of Minnesota, Minneapolis, MN 55455

Contributed by Britton Chance, December 16, 2004

We demonstrate that synthetic soft materials can extend the utility of natural vesicles, from predominantly hydrophilic reservoirs to functional colloidal carriers that facilitate the biomedical application of large aqueous-insoluble compounds. Near-infrared (NIR)-emissive polymersomes (50-nm- to 50-μm-diameter polymer vesicles) were generated through cooperative self assembly of amphiphilic diblock copolymers and conjugated multi(porphyrin)-based NIR fluorophores (NIRFs). When compared with natural vesicles comprised of phospholipids, polymersomes were uniquely capable of incorporating and uniformly distributing numerous large hydrophobic NIRFs exclusively in their lamellar membranes. Within these sequestered compartments, long polymer chains regulate the mean fluorophore–fluorophore interspatial separation as well as the fluorophore-localized electronic environment. Porphyrin-based NIRFs manifest photophysical properties within the polymersomal matrix akin to those established for these high-emission dipole strength fluorophores in organic solvents, thereby yielding uniquely emissive vesicles. Furthermore, the total fluorescence emanating from the assemblies gives rise to a localized optical signal of sufficient intensity to penetrate through the dense tumor tissue of a live animal. Robust NIR-emissive polymersomes thus define a soft matter platform with exceptional potential to facilitate deep-tissue fluorescence-based imaging for *in vivo* diagnostic and drug-delivery applications.

porphyrin | vesicles | nanoscale | diblock copolymer

Supramolecular self assembly has revolutionized soft materials research by enabling the efficient and high-throughput fabrication of complex multicomponent nanostructures (1–3). For decades, self-assembled vesicles comprised of phospholipids (liposomes) or small-molecule surfactants (4) have been used for sequestering high concentrations of hydrophilic compounds (5) and controlling their temporal release and distribution for maximal therapeutic efficacy (6). More recently, amphiphilic peptides and polymers have been shown to form very elaborate architectures (7–9) and serve as useful nanocontainers in aqueous solution (10). In particular, self-assembled materials are ideal for carrying promising imaging and therapeutic agents whose biomedical utility has hitherto been hampered by inadequate aqueous solubility (11). Here, we demonstrate the unique ability of synthetic amphiphiles to assemble into functional vesicles that membrane-disperse numerous large hydrophobic fluorophores and enable their specialized application for deep-tissue fluorescence-based *in vivo* imaging.

Although visible probes enable exquisite imaging of live animals by intravital microscopy (12), their utility is significantly limited at greater than submillimeter tissue depths as a result of extensive light scattering and optical absorption. Because light scattering diminishes with increasing wavelength, and hemoglobin electronic and water vibrational overtone absorptions approach their nadir over the near-infrared (NIR) spectral domain (700–950 nm) (13), considerable effort has been spent developing *in vivo* imaging platforms that use NIR light (14–17). Although significant progress has been made in constructing target-specific and locally active NIR-emissive probes (18–22), the development of biocompatible contrast agents of appropriate sensitivity remains a major technological hurdle for the realization of deep-tissue fluorescence-based imaging.

In general, the magnitude of any fluorescent signal will depend upon the local fluorophore concentration, the emission dipole strength per fluorophore, and the degree of local excitation. Such emissive signals will be attenuated by chromophore–chromophore and chromophore–local environment interactions that introduce additional nonradiative decay pathways or give rise to new low-lying nonemissive electronic states. Hence, optimizing fluorophore photophysics, regulating the average fluorophore–fluorophore interspatial separation, and delivering an appropriately large payload of emitters to a specific site are all challenges that must be addressed when designing new photonic beacons for *in vivo* imaging. We demonstrate that NIR-emissive polymersomes, vesicles comprised of amphiphilic diblock copolymers and large-emission dipole-strength NIR fluorophores (NIRFs) (Fig. 1), define a composition of soft matter that meets simultaneously all of these demands.

In our studies, the NIRFs derive from an oligo(porphyrin) structural motif that features cylindrically π symmetric bridging units, such as ethyne and butadiyne, that directly link juxtaposed (porphinato)zinc(II) (PZn) macrocycles (23–26). This mode of PZn-to-PZn connectivity modulates ground- and excited-state interchromophore electronic interactions, enabling predictable tuning of the fluorescence emission energy of these chromophores over a large window of the visible and NIR spectra (600–950 nm). In particular, PZn_2–PZn_5 hold promise as exogenous contrast enhancement agents for deep-tissue optical imaging (22). They possess large NIR emission dipole strengths and substantial radiative rate constants, as well as low-energy high-oscillator strength absorptive transitions that are ideally suited for facile NIR excitation (25). Although these chromophores possess highly attractive spectral characteristics, their size and rigid hydrophobic nature underscore the need for an appropriate amphipathic delivery vehicle.

Polymersomes, self-assembled vesicles comprised of amphiphilic diblock copolymers (27–29), demonstrate numerous properties in common with liposomes, their lipid counterparts; for example, both classes of bilayered vesicles are capable of encapsulating hydrophilic compounds in their aqueous core. Polymersomes, however, also exhibit several uniquely distinguishing characteristics: (*i*) augmented chemical stability due to their polyethylene-oxide (PEO) head groups confers biocompatibility, structural integrity in plasma, and "stealth"-like character resulting in long *in vivo* circulation times (30); and (*ii*)

Abbreviations: NIR, near infrared; NIRF, NIR fluorophore; PZn, zinc porphyrin [(porphinato)zinc(II)]; PEO, polyethylene-oxide; PBD, polybutadiene.

¶To whom correspondence may be addressed. E-mail: hammer@seas.upenn.edu or therien@sas.upenn.edu.

www.pnas.org/cgi/doi/10.1073/pnas.0409394102

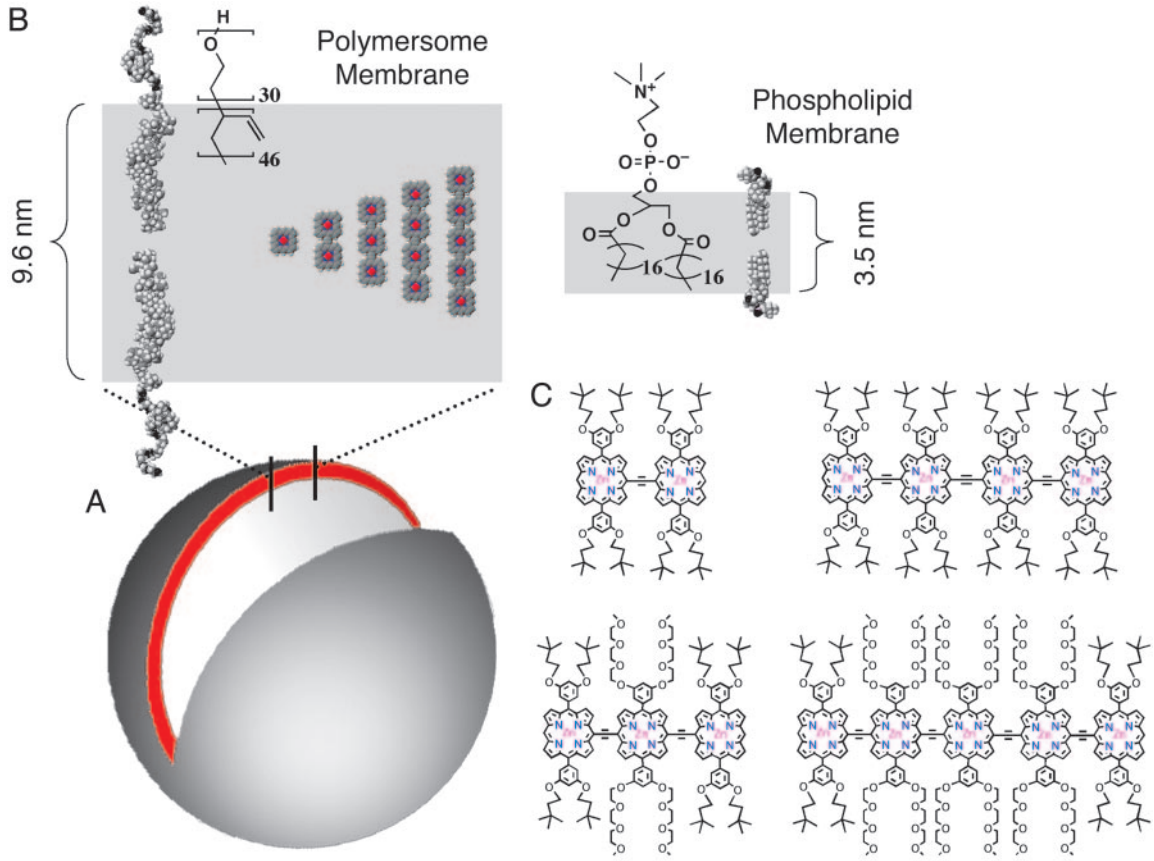

Fig. 1. Schematic representations of NIR-emissive polymersomes. (*A*) In aqueous solution, amphiphilic diblock copolymers of PEO_{30}-PBD_{46} self assemble into polymer vesicles (polymersomes) with the hydrophobic PBD tails orienting end-to-end to form bilayer membranes. The depicted unilamellar polymersome displays an excised cross-sectional slice illustrating the bilayer PBD membrane (gray) containing the hydrophobic PZn-based NIRFs (red). (*B*) CAChe-generated sectional schematic of the NIR-emissive polymersome membrane indicating the molecular dimensions of (*i*) the PBD component of the bilayer (9.6 nm); (*ii*) the large, dispersed PZn-based NIRFs (2.1 to 5.4 nm); and (*iii*) a typical liposome membrane (3–4 nm) comprised of phospholipids [1-stearoyl-2-oleoyl-sn-glycero-3-phosopho-choline (SOPC)]. (*C*) Chemical structures of NIRFs PZn_2–PZn_5.

depending upon the structure of their component copolymer blocks, polymersome membranes are also significantly thicker (≈9–22 nm) than those of liposomes comprised of natural phospholipids (3–4 nm) (Fig. 1*B*) (31). These synthetic lamellar membranes possess enormous mechanical strength that makes polymersomes 5–50 times tougher than liposomes (32) and substantially more stable than micellar structures constructed from similar molecular weight copolymers [e.g., critical surface tension of ≈120 (32) vs. ≈50 mN/m (33) for ≈4,000 M_r amphiphilic diblock].

Here, we explore the ability of the thick polymersome membrane to stably incorporate large multimeric porphyrin-based NIRFs and to uniquely enable their specialized biomedical application; these di-, tri-, tetra-, and penta-PZn structures (PZn_2–PZn_5: ranging 2.1–5.4 nm in length and 1.8–5.4 M_r; Fig. 1*C*) possess a *meso*-to-*meso* ethyne-bridged linkage and span peak emission wavelengths of 723, 809, 867, and 900 nm, respectively, within the polymersomal matrix.

Materials and Methods

NIRF Incorporation into Polymersome Membranes by Thin-Film Rehydration. One hundred microliters of 1 mM PEO_{30}– PBD_{46} diblock copolymer (Polymer Source, Dorval, PQ, Canada) solution and 5 μl of 1 mM solution of NIRF species (PZn_2–PZn_5) in methylene chloride were uniformly coated on the inside wall of a glass vial or on the surface of roughened Teflon, followed by evaporation of the solvent under vacuum for >12 h. Addition of sucrose solution (250–300 milliosmolar) and heating at 60°C for 24 h lead to spontaneous budding of giant (5–50 μm) NIR-emissive polymersomes (membrane loaded at a molar ratio of 20:1 polymer/NIRF) off of the glass (or Teflon) into the aqueous surroundings.

Small (<300-nm diameter) unilamellar polymersomes that possess appropriately narrow size distributions were prepared via procedures analogous to those used to formulate small lipid vesicles (sonication, freeze-thaw extraction, and extrusion). The sonication procedure involved placing a sample vial containing the aqueous-based solution and a dried thin-film formulation (of polymer and NIRF species uniformly deposited on Teflon) into a bath sonicator (Fischer Scientific; Model FS20) with constant agitation for 30 min. Five cycles of freeze–thaw extraction followed by placing the sample vials (containing solutions of medium-sized 300-nm NIR-emissive polymersomes) in liquid N_2. Once the bubbling from the liquid N_2 subsided, the vials were subsequently transferred to a 56°C water bath. Extrusion to a monodispersed suspension of small (e.g., 100-nm diameter) vesicles proceeded by introduction of the polymersome solution into a thermally controlled stainless steel cylinder connected to pressurized nitrogen gas. The solution was pushed through a 0.1-μm polycarbonate filter (Osmonics, Livermore, CA) supported by a circular steel sieve at the bottom of the cylinder, where the vesicles were collected after extrusion. This procedure was repeated multiple times, and the size distribution of polymersomes was measured by

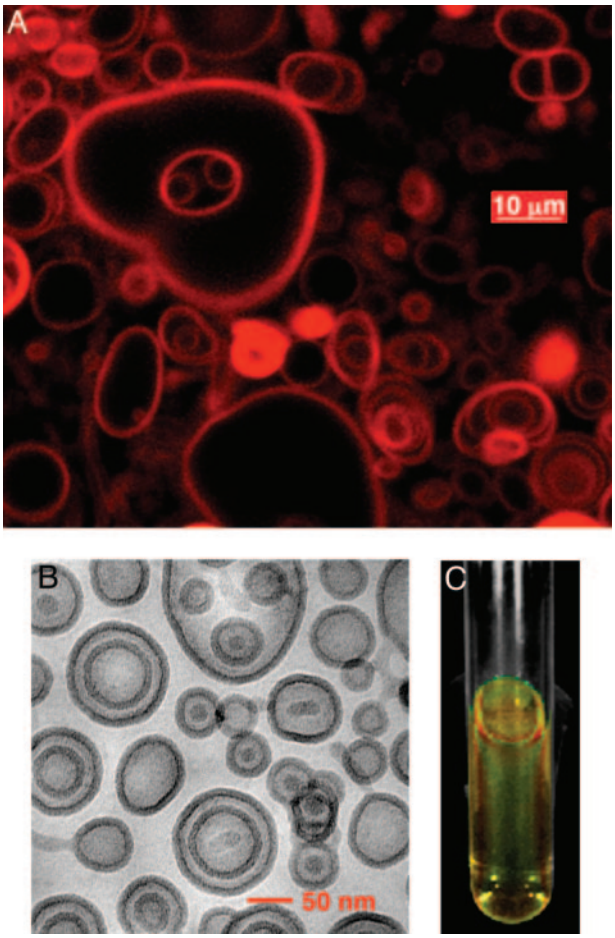

Fig. 2. Confocal and *in situ* fluorescence imaging of NIR-emissive polymersomes. (*A*) Scanning fluorescence confocal microscope image (λ_{em}^{max} = 809 nm) of 5- to 50-μm polymer vesicles featuring membrane-dispersed NIRF PZn_3 loaded at 5 mol% concentration. (Bar, 10 μm.) (*B*) Cryogenic transmission electron microscope (cryo-TEM) image of 50- to 150-nm PZn_3-loaded NIR-emissive polymersomes produced by sonication and freeze–thaw extraction of a dry thin film formulation of polymer and NIRF. A mono-dispersed suspension of unilamellar vesicles was further achieved after extrusion through a pressurized membrane. (*C*) *In situ* fluorescence image of a 10-ml sample tube containing 5 ml of a mono-dispersed aqueous suspension of small (<100-nm) unilamellar PZn_3-based NIR-emissive polymersomes. The image was obtained with a Xenogen Ivis Imaging System equipped with a charge-coupled device-based camera and appropriate filters for specific NIR excitation and fluorescence detection.

dynamic light scattering (DynaPro, Protein Solutions, Charlottesville, VA).

Confocal Microscopy of NIR-Emissive Polymersomes. Giant (5- to 50-μm) NIR-emissive polymersomes in 290 milliosmolar sucrose were fabricated by the methods described above. Vesicle solutions were diluted 30:70 in osmotically matched PBS. Fluorescence scanning confocal microscope images were obtained by using a Radiance 2000 Multiphoton Confocal System (Bio-Rad) equipped with a 650-nm long-pass emission filter (excitation via argon laser, λ_{ex} = 488 nm). Fig. 2*A*, demonstrating fluorescence emission from NIRF PZn_3-based NIR-emissive polymersomes, was modified for contrast and brightness by using PHOTOSHOP software (Adobe Systems, San Jose, CA).

Photophysical Studies of NIR-Emissive Polymersome Solutions. Medium-sized (300-nm) NIR-emissive polymersomes were generated by thin-film rehydration and sonication; electronic absorption and fluorescence spectrophotometric studies of the aqueous vesicle solutions were conducted to obtain data on incorporation efficiencies and fluorescence properties.

The aqueous vesicle solutions (n = 10 for each PZn_2-PZn_5-based polymersome formulation) were placed in 10-mm quartz optical cells, and electronic absorption spectra for each of the membrane-incorporated NIRF species were recorded on an OLIS UV/Vis/NIR spectrophotometry system that is based on the optics of a Cary 14 spectrophotometer (On-Line Instruments). Two milliliters of each aqueous vesicle solution were then transferred to a glass vial and frozen in liquid N_2. Next, the frozen solutions were lyophilized (FreeZone 4.5 L Benchtop Freeze Dry System, Labconco, Kansas City, MO; Model 77500) for 24 h to destroy the vesicles and dry the polymer and NIRF species. The dry samples were then taken up in the same volume of tetrahydrofuran (THF), and their absorption spectra were recorded. The concentrations of PZn_2–PZn_5 in the original polymersome solutions were calculated via Beer's law by using the absorption spectra taken in THF and the previously determined average molar extinction coefficients (ε, $M^{-1}\cdot cm^{-1}$) for the emitters in this solvent (25). These calculated concentrations, as well as the original NIRF absorption spectra in aqueous polymersome solutions, were used to determine the ε for PZn_2–PZn_5 loaded in the vesicle membranes.

Fluorescence spectra of NIR-emissive polymersomes were obtained with a Spex Fluorolog-3 spectrophotometer (Jobin Yvon, Edison, NJ) that used a dual S and T channel configuration and PMT/InGaAs/Extended-InGaAs detectors (λ_{ex} = 510 nm). Emission spectra were corrected by using the spectral output of a calibrated light source supplied by the U.S. National Bureau of Standards.

Direct Tumor Injection of NIR-Emissive Polymersomes in a Live Animal. Rat 9L glioma tumor cells were implanted on the right flank of a male Fisher 344 rat (200 g) via s.c. injection of 0.1 ml of saline containing $\approx 10^6$ glioma cells. Within 14 days, the tumor grew to the size of 2 cm in diameter. After a 24-h fast, the rat was anesthetized via 1.5-ml i.p. injection [83.3% ketamine (75 mg/kg), 5.55% xylazine (10 mg/kg), and 11.1% saline]. Approximately 20 μg of NIR-emissive polymersomes, membrane loaded to 5 mol% PZn_3, in 100 μl of 0.9% Sodium Chloride Injection USP (Abbott) were then introduced via direct injection into the center of the 2-cm-diameter s.c. tumor.

***In Vivo* Fluorescence Imaging of NIR-Emissive Polymersomes.** Fluorescence images of NIR-emissive polymersomes, generating a signal from deep within the tumor of a live animal, were obtained by using an Ivis Imaging System (Xenogen, Alameda, CA; 100 series) equipped with white-light excitation, charge-coupled device camera-based fluorescence detection, and a filter set appropriate for NIR-emitting indocyanine green (band-pass excitation 705–765 nm and emission 805–880 nm). Successive images were taken at t = 0, 5, 10, 15, and 20 min after direct tumor injection of the NIR-emissive polymersome solution. The animal was then killed, and the tumor was imaged by using a high-resolution fluorescence scanner.

High-Resolution *ex Vivo* Fluorescence Imaging of NIR-Emissive Polymersomes. Low-temperature 3D fluorometric scanning was used to provide greater spatial resolution of the NIR-emissive polymersome signal emanating from deep within the tumor. A snap-freeze clamping technique was used to control the metabolic state of the tissue and to keep it constant for subsequent fluorescence measurements. The animal was immersed in precooled isopentane (−150°C) for 5 min and subsequently transferred to liquid nitrogen (−196°C). The tumor was then

surgically excised, embedded in a mixture of ethanol–glycerol–water (10:30:60; freezing point: −30°C), and mounted at low temperature for high-resolution fluorescence imaging via a 3D surface scanning optical system (34). The resolution in the Z direction was 10 μm above the surface of the shaved sample. The fluorescence signal was automatically digitized and recorded on a personal computer, and the 3D tumor image was generated with MATLAB software (Mathworks, Natick, MA).

Results and Discussion

Generation of NIR-Emissive Polymersomes in Micro- and Nanometer Dimensions. The vesicles are formed through cooperative self assembly of amphiphilic diblock copolymers of PEO(1300)-b-1,2PBD(2500) (Fig. 1*B*) and large hydrophobic fluorophores PZn_2–PZn_5 (Fig. 1*C*). The polymer and NIRF species are deposited as a uniform thin film on Teflon, dried under vacuum, and then subjected to rehydration in aqueous solution. Upon gentle heating (60°C, 24 h), giant (5- to 50-μm) NIR-emissive polymersomes spontaneously bud off the Teflon film into the bulk solution. Standard methods established for liposomes (6) (sonication, freeze/thaw extraction, and extrusion) are used to yield mono-dispersed suspensions of unilamellar vesicles <100 nm in diameter.

Confocal Microscopy and Photophysical Characterization of NIR-Emissive Polymersomes. Confocal microscopy studies evince uniform dispersion of numerous emissive fluorophores sequestered within the polymersomes' membranes and demonstrate that the vesicles maintain an aqueous interior free of dye with potential for hetero-functional utility (Fig. 2*A*). The membrane-specific accumulation of NIRFs is strongly driven by their hydrophobicity; hence there is no need for further solution processing after self assembly (e.g., removal of unincorporated dye or purification of the polymersome product to homogeneous composition). There is also no detectable leakage of NIRFs to the external aqueous solution or internal core, nor is there a decrease in vesicle stability over a timescale of weeks. Due to facile self assembly of these soft matter structures, scale-up is readily achieved to yield quantities of nanometer-sized NIR-emissive polymersomes suitable for *in vivo* imaging applications (Fig. 2 *B* and *C*; see below).

Because porphyrin aggregation results in interchromophoric interactions that favor processes (e.g., self absorption and augmentation of nonradiative decay channels) that attenuate fluorescence, both segregation of the fluorophores and control of their microenvironment are imperative. Spectrophotometric analyses of aqueous solutions of NIR-emissive polymersomes verify strong absorption and fluorescence emission from large numbers of membrane-soluble NIRFs, indicating excellent fluorophore dispersion and light-harvesting characteristics (Fig. 3*A*). Porphyrin-based NIRFs manifest photophysical properties within the polymersomal matrix that are similar to those previously established in organic solvents. Polymersomes further prove capable of incorporating a comprehensive range of related ethynyl- and butadiynyl-bridged bis- and tris(porphinato)zinc NIRFs (see supporting information, which is published on the PNAS web site), affording the ability to precisely tune the peak emission wavelength of the assembly anywhere in the 600- to 950-nm range of the visible and NIR spectral domains (Fig. 3*B*). NIR-emissive polymersomes (membrane loaded at >5 mol% NIRF/polymer) can be fabricated for even the largest porphyrin-based fluorophores (PZn_5).

Table 1. NIRF copy number per PZ_{n_3}-based vesicle, reported as a function of polymersome size for a 5 mol% membrane loading

Polymersome size	Example	No. of copies of NIRF
Small (<300 nm)	100 nm	2,500
Medium (300 nm–1 μm)	500 nm	75,000
Giant (>1μm)	1 μm	300,000

Computations assume a 1-nm^2 projected area per PBD block composing the polymersome's bilayer membrane (31).

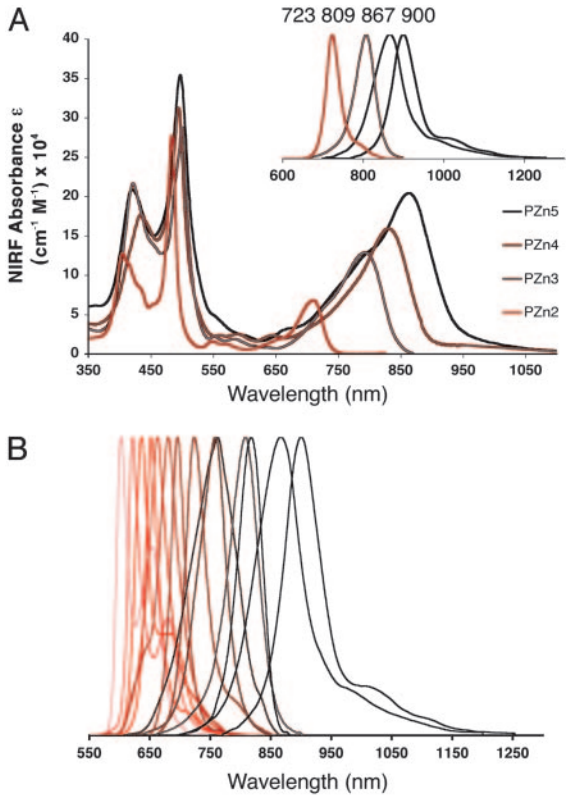

Fig. 3. Absorbance and emission spectra of aqueous solutions of NIR-emissive polymersomes. (*A*) Aqueous absorption and emission (*Inset*) spectra of emissive polymersomes containing NIRFs (*i*) PZn_2, (*ii*) PZn_3, (*iii*) PZn_4, and (*iv*) PZn_5. [Experimental conditions: λ_{ex} = 510 nm. Note that these complexes possess subps S_2-to-S_1-state internal conversion times; hence, visible electronic excitation gives rise, with unit quantum efficiency, to the identical low-energy-emitting state that is accessed via NIR excitation (26).] Increasing conjugation length in PZn_2–PZn_5 augments the NIR absorption oscillator strength and shifts both the fluorophore absorption and corresponding emission maxima progressively to longer wavelengths (23–26). (*B*) Demonstration of facile fluorescence-wavelength modulation of vis- and NIR-emissive polymersomes. Emission bands of PZn_2–PZn_5 (*A*) are reproduced; other emission bands shown derive from polymersomes incorporating related ethynyl- and butadiynyl-bridged NIRFs (Table 2) (23, 24).

Analogous experiments that examine NIRF loading in liposomes indicate that membrane incorporation of a benchmark PZn monomer (PZn_1) and PZn_2 can be achieved only at loading levels approaching 1 mol% (see supporting information). That no observable quantity of longer-wavelength emitting PZn_3–PZn_5 can be incorporated within liposomes stems from the fact that the lengths of these species (3.2–5.4 nm) approach or exceed the thickness of conventional lipid membranes (≈3.5 nm). In contrast, PZn_3–PZn_5 are of relatively small size when compared with the thickness of the polymersome bilayer membrane (9.6 nm) (31) and lead to little or no alteration in the membrane structure upon their noncovalent incorporation. Note that a single 100-nm-diameter polymersome, a size appropriate for many *in vivo* imaging applications

(35), carries ≈2,500 copies of a NIR-emitting fluorophore, as calculated for a corresponding 5 mol% membrane loading (Table 1). The vesicular volume element thus possesses an emitter concentration of ≈3 mM. Moreover, in aqueous solution, for such a 100-nm-sized emissive polymersome incorporating PZn_3, 5 mol% loading corresponds to a vesicular molar absorptive extinction coefficient of $3.2 \times 10^8\ M^{-1}\cdot cm^{-1}$ (λ = 794 nm). Steady-state emission spectroscopy further establishes that this loading level maximizes the emission intensity of PEO_{30}–PBD_{46}-based polymersomes (see supporting information).

***In Vivo* and *ex Vivo* Optical Imaging of NIR-Emissive Polymersomes.** The ability to uniformly disperse large numbers of high-emission dipole strength NIRFs PZn_2–PZn_5 within the polymer bilayer membrane, coupled with the capacity to reliably engineer polymersome size distributions, suggests the development of soft macromolecular optical materials suitable for biomedical application. In preparation for more extensive *in vivo* imaging studies, we conducted several proof-of-principle experiments to determine the sensitivity as well as the photo- and chemical stability of NIR-emissive polymersomes in physiological environments. First, we tested their ability to generate a localized optical signal of sufficient intensity to penetrate through a dense tumor of a live animal. A 9L glioma-bearing rat was imaged at various time points after direct tumor injection of 100 μl of saline containing ≈20 μg of 300-nm-sized NIR-emissive polymersomes (membrane loaded at 5 mol% with PZn_3; ≈500 pmol total NIRF). The fluorescence signal emanating from the live animal was monitored by using a CCD-based camera and Xenogen Imaging system equipped with NIR excitation and emission filters (Fig. 4*A*). The animal was then killed, and the tumor was subsequently imaged *ex vivo* with a high-resolution ($80 \times 80 \times 10\ \mu m^3$) 3D scanning optical imaging system (34) to corroborate the localization of the emissive signal within the tumor.

Fig. 4*A* illustrates intense highly localized fluorescence after vesicle injection to a tissue depth of 1 cm below the skin surface. Higher-resolution 3D optical scanning of the same tumor further demonstrated a signal-to-background ratio of at least 10:1 (Fig. 4*B*). Notably, the signal intensity at this concentration and depth of emitters is qualitatively similar to that reported recently in an *in vivo* study by using type II quantum dots (400 pmol at 1-cm depth) (36). Like their inorganic counterparts, NIR-emissive polymersomes also demonstrated a high photobleaching threshold in aqueous solution (>500 mW/cm^2 under continuous laser illumination for 20 min; see supporting information). Moreover, the vesicles were chemically stable in physiological environments, as evidenced by their constant fluorescence signal intensity when monitored in 37°C plasma for 1 wk (see supporting information). These results indicate that *in vivo*, NIRF-incorporated polymersomes are emissive and do not undergo substantial phase transitions that drive porphyrin aggregation or facilitate intermembranous fluorophore transfer to surrounding biological structures.

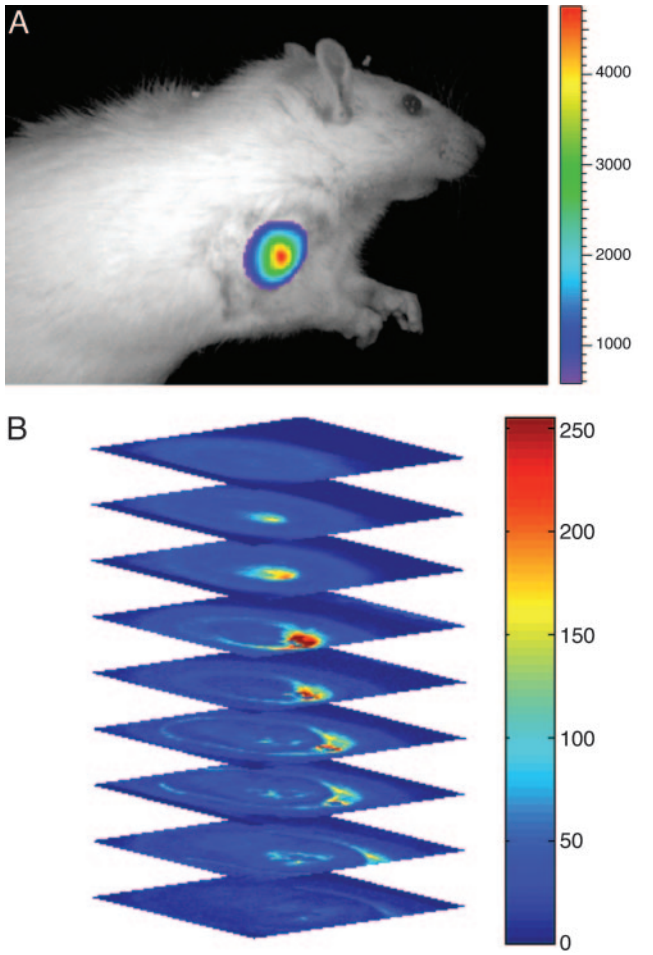

Fig. 4. *In vivo* and *ex vivo* optical imaging of NIR-emissive polymersomes. (*A*) *In vivo* fluorescence image of 300-nm-sized NIR-emissive polymersomes (membrane loaded at 5 mol% with PZn_3; ≈500 pmol total NIRF) taken 10 min after direct tumor injection of a 9L glioma-bearing rat. The fluorescence signal intensity corresponded to only half the integrated emission from the vesicles, and it remained constant between successive images taken during a 20-min interval postinjection (image: maximum counts = 47,309, minimum counts = 361.54; Bar, maximum counts = 47,309, minimum counts = 5,874). (*B*) High-resolution *ex vivo* 3D fluorescence scanning of the same tumor via a low-temperature optical imaging system (34). The maximally bright signal (red), in the minimally fluorescent background of tumor (blue), corresponds to a >10-fold signal enhancement emanating from NIR-emissive polymersomes located at a 1-cm tissue depth.

Conclusion

NIR-emissive polymersomes are self-assembled multicomponent macromolecular structures that are well suited for deep-tissue optical imaging. The stability of these synthetic vesicles, coupled with the ability to modulate their emission over a 600- to 950-nm wavelength domain, defines a family of nanometer-sized emissive soft matter that offers an intriguing complement to *in vivo* imaging platforms based on quantum dots (36). Moreover, given the ubiquitous nature of porphyrinoid pigments in biology and the possibility to use biodegradable amphiphilic block copolymers (37–41), these versatile, biocompatible vesicles (30) also have the potential to be made fully bioresorbable. Finally, the self-assembled vesicular architecture allows for the economic and facile generation of complex colloids based on a biomimetic template. Compartmentalization of targeting molecules (via surface conjugation to PEO head groups) (42), imaging compounds (segregated in the membrane), and therapeutics (dissolved in the aqueous vesicular interior) should enable the evolution of polymersomes into multimodality agents. NIR-emissive polymersomes thus exemplify the enormous capability of soft matter self assembly to yield functional colloids that facilitate the novel biomedical application of their molecular components.

We are grateful to Dr. W. S. El-Deiry for the use of his Xenogen Imaging System. M.J.T. and D.A.H. thank the Materials Research Science and Engineering Center Program of the National Science Foundation (Grant DMR-00-79909) for infrastructural support. D.A.H. also thanks the National Institutes of Health (Grant EB003457-01), and P.P.G. acknowledges fellowship support from the National Institutes of Health Medical Scientist Training Program and the Whitaker Foundation. This work was supported by National Cancer Institute Grant R33-NO1-CO-29008.

1. Stupp, S. I., LeBonheur, V., Walker, K., Li, L. S., Huggins, K. E., Keser, M. & Amstutz, A. (1997) *Science* **276,** 384–389.
2. Hamley, I. W. (2003) *Angew. Chem. Int. Ed.* **42,** 1692–1712.
3. Kimizuka, N. (2003) *Curr. Opin. Chem. Biol.* **7,** 702–709.
4. Kaler, E. W., Murthy, A. K., Rodriguez, B. E. & Zasadzinski, J. A. N. (1989) *Science* **245,** 1371–1374.
5. Bangham, A. D., Standish, M. M. & Watkins, J. C. (1965) *J. Mol. Biol.* **13,** 238.
6. Torchilin, V. P. & Weissig, V. (2003) in *Practical Approach Series* (Oxford Univ. Press, Oxford), Vol. 264, pp. 1–396.
7. Deming, T. J. (1997) *Nature* **390,** 386–389.
8. Dinsmore, A. D., Hsu, M. F., Nikolaides, M. G., Marquez, M., Bausch, A. R. & Weitz, D. A. (2002) *Science* **298,** 1006–1009.
9. Jain, S. & Bates, F. S. (2003) *Science* **300,** 460–464.
10. Zhang, S. G., Marini, D. M., Hwang, W. & Santoso, S. (2002) *Curr. Opin. Chem. Biol.* **6,** 865–871.
11. Langer, R. (1998) *Nature* **392,** 5–10.
12. Jain, R. K., Munn, L. L. & Fukumura, D. (2002) *Nat. Rev. Cancer* **2,** 266–276.
13. Chance, B. (1998) *Ann. N.Y. Acad. Sci.* **838,** 29–45.
14. Franceschini, M. A., Moesta, K. T., Fantini, S., Gaida, G., Gratton, E., Jess, H., Mantulin, W. W., Seeber, M., Schlag, P. M. & Kaschke, M. (1997) *Proc. Natl. Acad. Sci. USA* **94,** 6468–6473.
15. Hawrysz, D. J. & Sevick-Muraca, E. M. (2000) *Neoplasia* **2,** 388–417.
16. Intes, X., Ripoll, J., Chen, Y., Nioka, S., Yodh, A. G. & Chance, B. (2003) *Med. Phys.* **30,** 1039–1047.
17. Weissleder, R. & Ntziachristos, V. (2003) *Nat. Med.* **9,** 123–128.
18. Weissleder, R., Tung, C. H., Mahmood, U. & Bogdanov, A., Jr. (1999) *Nat. Biotechnol.* **17,** 375–378.
19. Achilefu, S., Dorshow, R. B., Bugaj, J. E. & Rajagopalan, R. (2000) *Invest. Radiol.* **35,** 479–485.
20. Becker, A., Hessenius, C., Licha, K., Ebert, B., Sukowski, U., Semmler, W., Wiedenmann, B. & Grotzinger, C. (2001) *Nat. Biotechnol.* **19,** 327–331.
21. Zaheer, A., Lenkinski, R. E., Mahmood, A., Jones, A. G., Cantley, L. C. & Frangioni, J. V. (2001) *Nat. Biotechnol.* **19,** 1148–1154.
22. Sevick-Muraca, E. M., Houston, J. P. & Gurfinkel, M. (2002) *Curr. Opin. Chem. Biol.* **6,** 642–650.
23. Lin, V. S.-Y., DiMagno, S. G. & Therien, M. J. (1994) *Science* **264,** 1105–1111.
24. Lin, V. S.-Y. & Therien, M. J. (1995) *Chem. Eur. J.* **1,** 645–651.
25. Susumu, K. & Therien, M. J. (2002) *J. Am. Chem. Soc.* **124,** 8550–8552.
26. Rubtsov, I. V., Susumu, K., Rubtsov, G. I. & Therien, M. J. (2003) *J. Am. Chem. Soc.* **125,** 2687–2696.
27. Discher, B. M., Won, Y. Y., Ege, D. S., Lee, J. C. M., Bates, F. S., Discher, D. E. & Hammer, D. A. (1999) *Science* **284,** 1143–1146.
28. Discher, D. E. & Eisenberg, A. (2002) *Science* **297,** 967–973.
29. Antonietti, M. & Forster, S. (2003) *Adv. Mater.* **15,** 1323–1333.
30. Photos, P. J., Bacakova, L., Discher, B., Bates, F. S. & Discher, D. E. (2003) *J. Controlled Release* **90,** 323–334.
31. Won, Y. Y., Brannon, A. K., Davis, H. T. & Bates, F. S. (2002) *J. Phys. Chem. B.* **106,** 3354–3364.
32. Bermudez, H., Brannan, A. K., Hammer, D. A., Bates, F. S. & Discher, D. E. (2002) *Macromolecules* **35,** 8203–8208.
33. Riess, G. (2003) *Prog. Polymer Sci.* **28,** 1107–1170.
34. Gu, Y. Q., Qian, Z. Y., Chen, J. X., Blessington, D., Ramanujam, N. & Chance, B. (2002) *Rev. Sci. Instrum.* **73,** 172–178.
35. Moghimi, S. M., Hunter, A. C. & Murray, J. C. (2001) *Pharmacol. Rev.* **53,** 283–318.
36. Kim, S., Lim, Y. T., Soltesz, E. G., De Grand, A. M., Lee, J., Nakayama, A., Parker, J. A., Mihaljevic, T., Laurence, R. G., Dor, D. M., *et al.* (2004) *Nat. Biotechnol.* **22,** 93–97.
37. Jeong, B., Bae, Y. H., Lee, D. S. & Kim, S. W. (1997) *Nature* **388,** 860–862.
38. Meng, F. H., Hiemstra, C., Engbers, G. H. M. & Feijen, J. (2003) *Macromolecules* **36,** 3004–3006.
39. Najafi, F. & Sarbolouki, M. N. (2003) *Biomaterials* **24,** 1175–1182.
40. Bellomo, E. G., Wyrsta, M. D., Pakstis, L., Pochan, D. J. & Deming, T. J. (2004) *Nat. Mater.* **3,** 244–248.
41. Napoli, A., Valentini, M., Tirelli, N., Muller, M. & Hubbell, J. A. (2004) *Nat. Mater.* **3,** 183–189.
42. Lin, J. J., Silas, J. A., Bermudez, H., Milam, V. T., Bates, F. S. & Hammer, D. A. (2004) *Langmuir* **20,** 5493–5500.